Optics and Laser Technology 128 (2020) 106159

Contents lists available at ScienceDirect

Optics and Laser Technology

journal homepage: www.elsevier.com/locate/optlastec

Engineering of high quality factor THz metasurfaces by femtosecond laser ablation

Gian Paolo Papari[a,b,*], Jijil J.J. Nivas[a,b], Can Koral[c], Elaheh Allahyari[a,b], Salvatore Amoruso[a,b], Antonello Andreone[a,b,c]

[a] Dipartimento di Fisica, Università di Napoli "Federico II," via Cinthia, I-80126 Napoli, Italy
[b] CNR-SPIN, UOS Napoli, via Cinthia, I-80126 Napoli, Italy
[c] INFN Napoli Unit, via Cinthia, I-80126 Napoli, Italy

HIGHLIGHTS

- Metasurfaces can be realized employing laser ablation as fabrication technique.
- Transmission of metasurfaces present resonances with high quality factor.
- Full wave simulations show a very high control of transmission characteristics.

ABSTRACT

We report on the realization of high Q metasurfaces operating in the THz frequency range by femtosecond laser ablation applied to a nanometric metallic layer over a silicon substrate. Two different fabrication methods are used to develop periodic patterns whose basic elements are in form of an array of through-holes or metallic islands. The response of the resulting structures is characterized using a time-domain spectrometer in the frequency range 0.3–1.5 THz. The experimental findings are compared with the predictions of full wave electromagnetic simulations. The fairly good agreement between simulation predictions and experimental findings evidences that the proposed approach can offer a facile way to the elaboration of THz metasurfaces.

1. Introduction

A metasurfaces (MS) is a two-dimensional artificial material whose electromagnetic (e.m.) response is determined by design, depending on both the geometrical features of a unit cell (UC) – that plays the role of a "meta-atom" - and the periodic spatial arrangement of the UCs themselves [1–3]. A MS consists of a structured dielectric, semiconducting or conducting layer deposited on a low loss insulating substrate. In the limit of large wavelengths, a MS behaves as a homogeneous material with engineered electrodynamic properties. Thus, a MS can be designed to manipulate the impinging light to realize, for instance, elements showing selective absorption [4], beam steering [5] or super focusing properties [6], polarization converters [7], or to control the overall dielectric function of a sample [8,9].

Depending on the frequency range of operation the UCs of a MS can be realized resorting to a number of different techniques. UV [10] and soft lithography [11] are usually used when line resolution of a few micrometers is required. This applies to MSs operating in the THz frequency range (0.1–10.0 THz), since they have unit cell sizes of tens of micrometer [12,13].

Femtosecond Laser Ablation (FLA) is gaining interest as a fast and reliable fabrication method for 1- and 2-dimensional photonic crystals [14–17] and quasi-crystals [18,19], and recently MSs [20–26]. FLA is a versatile process since it does not need the usage of a photo-mask for the surface patterning. Specifically, it operates through selective removal or alteration of pre-determined areas from a conducting or dielectric layer juxtaposed over a substrate, leading to the realization of the MS through appropriate laser beam delivery strategies. In this paper we show that the electromagnetic response of different MSs can be tailored by applying FLA to a gold film deposited on silicon substrate. Full wave simulations provide the control on the MS realization along with the reproducibility of very high quality resonances.

2. Experimental techniques

In an attempt to extend previous works [20–22,24], we have fabricated various conducting MSs using the FLA process in two different configurations, as illustrated hereafter. The fabrication setup comprises

* Corresponding author.
E-mail address: gianpaolo.papari@unina.it (G.P. Papari).

https://doi.org/10.1016/j.optlastec.2020.106159
Received 22 October 2019; Received in revised form 16 January 2020; Accepted 24 February 2020
Available online 31 March 2020
0030-3992/

a Ti:Sa laser source (~35 fs, 800 nm, Gaussian spatial intensity distribution), a high precision three-axis stage for sample movement and an electromechanical shutter. The system is electronically controlled by in-house software that allows irradiating the sample surface at normal incidence with sequences of laser pulses in air. The sample is an Au film (thickness 180 nm) over an intrinsic (1 0 0) silicon substrate (thickness 400 μm). An intermediate CrNi layer (thickness 20 nm) is used to improve the Au film adhesion. The metallic thickness t is chosen to be larger than the skin depth (about 100 nm for gold at 1 THz [27]), so that the impinging radiation passes through a MS only via the ablated holes. Under this configuration MSs with sharp resonanμce features can be obtained.

Irradiation with a sequence of multiple fs pulses (typically between 2 and 5) is used to perforate the thin metallic film on the Si substrate. Controlled scanning of the sample under the beam allows exposing different areas in a predefined geometry realizing the final MS. This is done following two different procedures. In the first case, the laser beam hits the sample surface at some specific locations producing an array of circular holes. This array is replicated over a large area by step scanning, which allows the realization of a periodic pattern of the base array. This fabrication procedure realizes metagrids (MG) and is hereafter indicated as discrete mode (DM). In the second case, the laser is continuously scanned over the sample surface progressively removing "channels" of the metallic film, to realize a periodic pattern of conducting islands constituting the UCs of the MS. This second way is indicated as continuous mode (CM). DM is useful to produce diluted metals having a reduced plasma frequency, which is the "knob" for tuning the onset of surface plasmon polaritons [31,9], whereas CM allows realizing MS constituted by an array of micro-resonators. Laser repetition rates of 100 and 500 Hz, respectively, are used in the DM and CM procedures. Two different plano-convex lenses with focal length 35 mm and 75 mm are employed in the experiments and the value of the laser pulse energy, E_L, is appropriately selected to achieve the final dimensions of the structures. In the DM case, circularly polarized laser pulses are used to minimize any deformation in the circularity of the hole formed in the metallic film [9], while linear polarization is exploited for CM.

Various MS are realized and their THz response is analyzed by Time Domain Spectroscopy (TDS) exploiting a standard setup (Tera-K15, Menlo Systems). The technology is based on photo-conducting antennas (PCA) made of low temperature gallium arsenide (LT-GaAs), generating a transient electric field pulse of 1–2 ps when excited by a 90 fs pulsed laser at 1560 nm. Signals are acquired over a time scale of about 220 ps guaranteeing a frequency resolution of about 2.5 GHz. Experiments are performed in a dry nitrogen controlled environment to reduce unwanted water vapor peaks in the frequency spectrum. The linearly polarized beam is collimated using TPX lenses before impinging on the MS, so that one can safely assume an incident plane wave approximation. In the following we will refer to the system of coordinate as in Fig. 1 for the orientation of polarization, with x and y axes corresponding to horizontal and vertical directions, respectively. In particular, Fig. 1(a) reports a sketch of the UC of a representative sample (MG3, see below) and the incident electric field polarized along the vertical y-axis. Fig. 1(b) shows the corresponding THz signal vs time, where the dotted line and the continuous curve represent the transmission signals through MS and free space, respectively.

Table 1
MS geometrical parameters. $P_{x,y}$ is the UC periodicity in the plane. D represents the hole diameter of the MGs, whereas d_x (d_y) refers to the edge-edge distance along × (y) between adjacent holes (MG case) or rectangles (MS case).

Sample	P_X (μm)	P_Y (μm)	D (μm)	d_X (μm)	D_Y (μm)
MG1	190	190	77	113	113
MG2	180	180	37	8	8
MG3	180	180	37	8	8
MS1	186	123		64	66
MS2	186	78		63	62

Full-wave simulations of the signal are carried out using a commercial software for e.m. simulations (CST Microwave Studio). Periodic boundary conditions are set on the UC edges to mimic an infinite MS. The transmission coefficient $T = E_S/E_R$ of each MS is extracted from the ratio between the Fourier transform of the electric field passing through the sample (E_S) and the reference field (E_R) through the free space. The THz response of silicon is measured across a bare substrate, retrieving an average value of the complex dielectric function $\varepsilon_{Si} = 11.90 + i0.08$, with a negligible dispersion of the real part and a variation of the order of 10% for the imaginary part in the investigated spectral range.

3. Results and discussion

In the following, we illustrate the characteristic THz response of some selected samples, whose geometrical features are summarized in Table 1. Here, $P_{x,y}$ is the UC periodicity along the x- and y- directions; analogously, $d_{x,y}$ is the edge-edge distance between adjacent holes, for samples realized using the DM approach, and between adjacent rectangles, for samples realized using the CM approach (see below). In the case of metagrids, D represents the diameter of the single hole of the UC.

The corresponding optical images of these MSs are reported, as insets, in the panels of Figs. 2 and 3.

We consider first the MSs fabricated by DM, namely the MGs. In this case, each MS consists of a patterned metallic film with mutually connected UCs having a periodicity smaller than the excitation wavelength $\lambda = c/f$ [28,9], c being the speed of light and f the frequency. Under this condition, the MS behaves as a homogenous medium.

The sample MG1 is composed of a single array of holes with a diameter D = 77 μm and periodicity P = 190 μm (see inset in Fig. 2(a)). The holes of sample MG1 were realized by using laser pulses with an energy $E_L \approx 85$ μJ and the lens with 75 mm focal length. For the

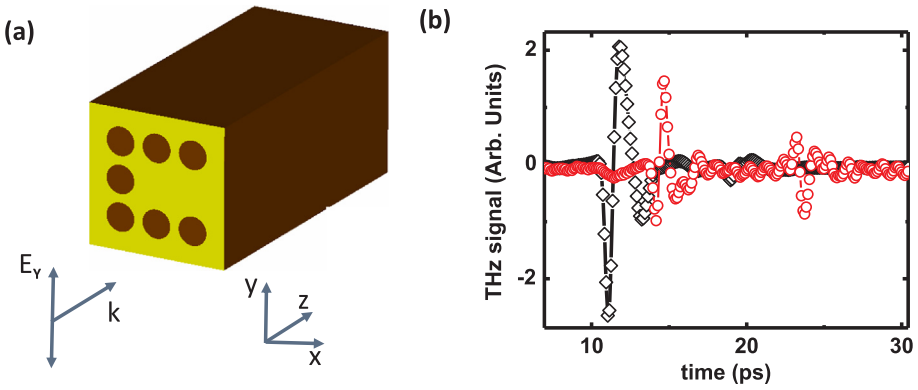

Fig. 1. (a) The sketch shows the UC of a representative sample (MG3) irradiated by a plane electromagnetic wave polarized along the (vertical) y-axis. (b) Amplitude of the corresponding signal transmission (dotted line) as a function of time. Black diamonds represent the reference signal passing through free space. The transmitted signal through MG3 is represented as red circles and it has been amplified by a factor 7 for easiness of comparison. (For interpretation of the references to colour in this figure legend, the reader is referred to the web version of this article.)

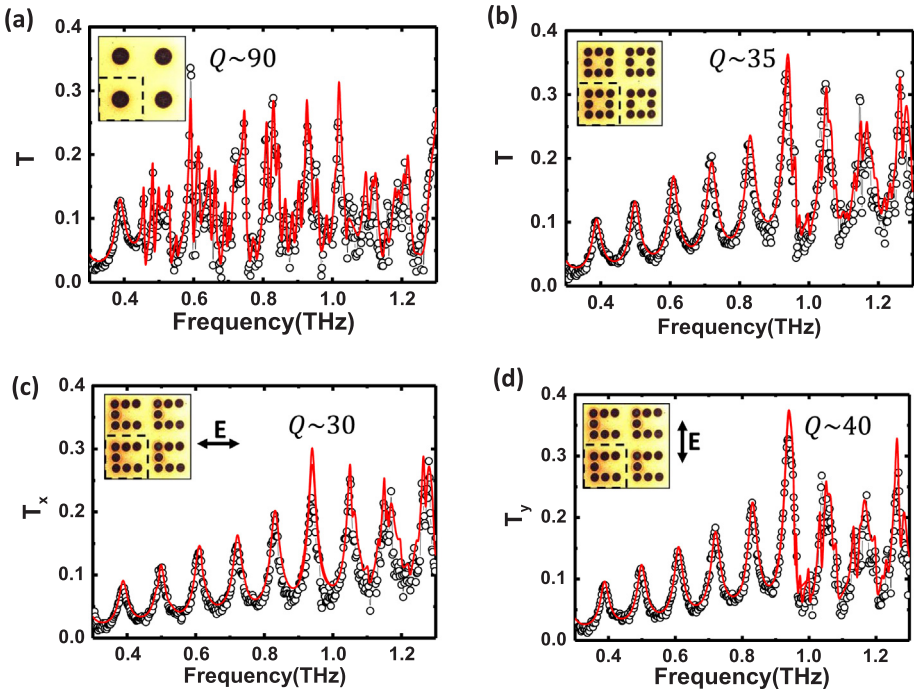

Fig. 2. Transmission coefficient for MG selected samples: (a) MG1, (b) MG2, (c) MG3 (y-polarization), (d) MG3 (x-polarization). The dots are the measurements whereas continuous red lines represent the full-wave e.m. simulations. In each panel the highest quality factor for the corresponding MS is reported (see text). Insets show a detailed view of the UC of each MG obtained by optical microscopy. The double headed arrow in panels (c) and (d) indicates the polarization of the impinging electric field. (For interpretation of the references to colour in this figure legend, the reader is referred to the web version of this article.)

sample MG2 the UC is formed by eight separated holes with D = 37 μm composing a square pattern (see inset in Fig. 2(b)) and the period is P = 180 μm. Finally, MG3 has the same geometrical parameters of MG2 but seven holes forming a UC arranged in a C-shaped structure (see insets of Fig. 2(c) and 2(d)). For the samples MG2 and MG3 laser pulses with an energy $E_L \approx 17$ μJ were focused on the sample with the lens having a focal length of 35 mm.

These MSs present enhanced transmission phenomena [29] manifesting themselves as peaks in the frequency spectrum. These maxima are triggered by impinging photons that couple with High Order Surface Plasmon Polaritons (HOSPP) mediating in such a way light tunneling across the MS [30]. For normal incidence transmission, each peak qualitatively fulfills the following cutoff relation:

$$f_{max} = \frac{c \bullet \sqrt{m_x^2 + m_y^2}}{P \bullet n_{eff}} \tag{1}$$

where $m_{x,y} = 0, 1, 2\cdots$ and

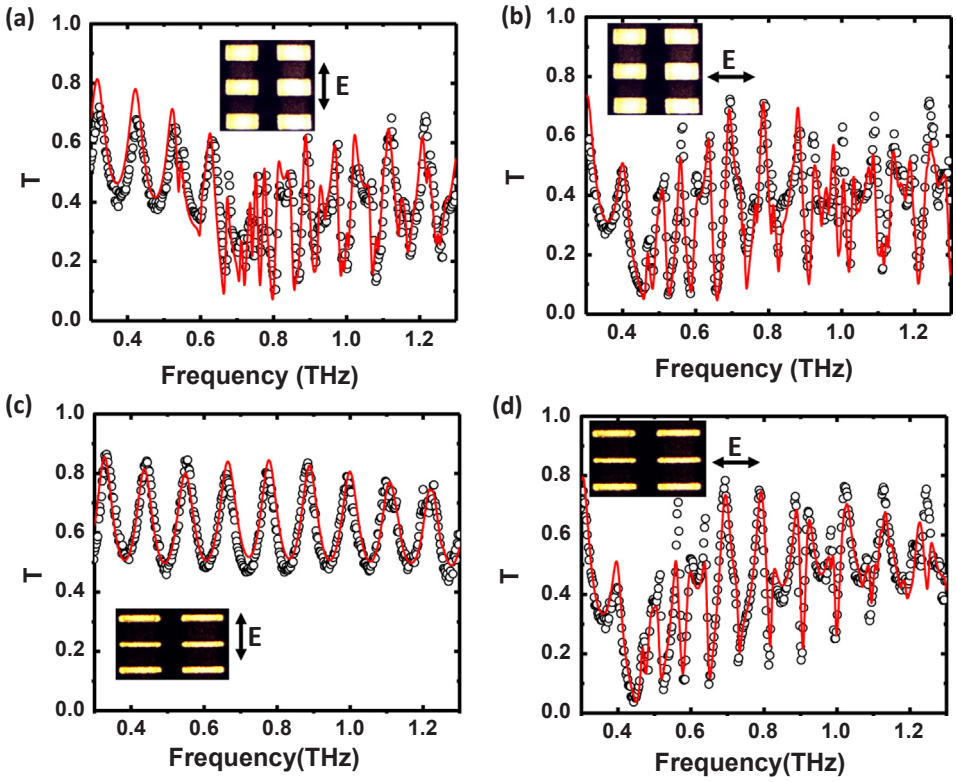

Fig. 3. Transmission *T* for vertical (y, left panels (a) and (c)) and horizontal (x, right panels (b) and (d)) polarizations for sample MS1 ((a), (b)) and sample MS2 ((c), (d)). In each panel the inset show an optical microscope image of the MS along with the polarization direction (double headed arrow) of the electric field E. Black dots are experimental data, while continuous curves represent the corresponding full wave-simulation results.

$$n_{eff} = Re\left\{\sqrt{\frac{\varepsilon_m \varepsilon_d}{\varepsilon_m + \varepsilon_d}}\right\} \quad (2)$$

is the effective refractive index at the interface between the metal, characterized by the complex function $\varepsilon_m = \varepsilon_m^{'} + i\varepsilon_m^{''}$, and the dielectric substrate, described by $\varepsilon_d = \varepsilon_d^{'} + i\varepsilon_d^{''}$.

The frequencies $f^1 \approx c/(P\sqrt{\varepsilon_d^{'}})$ and $f_D = c/P$ identify the lower and upper limit respectively of the spectral band where the metagrid response fulfills the homogeneity condition, and the output radiation can be still considered a plane wave before entering the diffractive regime. The expression for f^1 is easily obtained through Eq. (1) with $m_{x,y} = 0, 1$ and $n_{eff} \approx \sqrt{\varepsilon_d^{'}}$, since $\varepsilon_d^{'} \ll \varepsilon_m^{'}$ [31]. Considering an average period P 185μm and using the extracted dielectric constant $\varepsilon_d^{'}$ for Si, we qualitatively get as first resonance mode f^1 0.47 THz and as diffraction frequency f_D 1.6 THz [32]. Hence, in order to study the enhanced transmission phenomena under homogeneity condition, we focus our attention in the 0.3–1.5 THz spectral range, reporting in Fig. 2 the experimental transmission coefficient T as dots. In each panel, the red continuous line represents the result of a full-wave e.m. simulation that reproduces the experimental data fairly well. In particular, Fig. 2(a) shows data for sample MG1, whose transmission, qualitatively speaking, displays the highest number of peaks/resonances in the band of interest, as a consequence of its highest number of symmetries [33]. Instead, samples MG2 and MG3 (see Fig. 2(b) and 2(c)-(d), respectively) show a similar number of resonances, but less than MG1 since their UCs differ just for a single hole, keeping the symmetry only for integer $\pi/2$ rotations in the x-y plane.

To find the full metamaterial regime of the presented band, one can simulate the transmission scattering parameter (S_{21}) of an isolated UC embedded in a waveguide made of a perfect conductor. For all samples, the cutoff frequency is approximately $f_{UC} = 0.8$ THz, corresponding to the value $c/2P$ valid for a waveguide. Therefore one can identify frequency intervals in a strong ($f^1 < f < f_{UC}$) or weak ($f_{UC} < f < f_D$) metamaterial regime according to the onset of single UC modes. This behavior explains why resonance peaks beyond f_{UC} are more robust, as clearly shown in Fig. 2.

It is worth noting that within the entire metamaterial band the MGs produced by FLA present the highest Q factors available in literature in the THz band [34,35]. In particular, the simplest MG1 shows in full metamaterial regime at 0.59 THz a ultra-high quality factor Q 90, whereas samples MG2 and MG3 display record values for the weak metamaterial band, spanning the range between 30 and 40. The relative error in the quality factor evaluation $\frac{\delta Q}{Q}$ is estimated to be of the order of 5%.

Moreover, in the case of sample MG3 the geometrical asymmetry can be exploited to create a dichroic response. At $f_Q = 0.9$ THz, for example, a drastic change in signal amplitude (about 50%) is measured depending on the field polarization. It is worth noticing that the dichroism of MG3, obtained through a $\pi/2$ rotation of the "C-shaped" UC with respect to the polarization direction of the impinging field, can be equivalently realized switching "on" and "off", with an external stimulus, the conductivity of the additional hole in sample MG2. This property might be exploited for the development of fast switches in THz optoelectronics.

We turn now to MSs fabricated by exploiting the CM approach. Applying the FLA process in the CM configuration, it is possible to realize similarly high performing optical devices. In particular, we consider here two MSs consisting of an array of conducting rectangles characterized by the geometrical parameters reported in Table 1, and exemplified in the optical images reported as insets in Fig. 3. The MSs were elaborated by using laser pulses with an energy $E_L \approx 20$ μJ focused by the lens with a focal length of 35 mm. Black dots in Fig. 3 (a)–(d) represent the experimental transmissions under x- and y-polarization, respectively, for the samples MS1 and MS2. The continuous lines in Fig. 3 represent the corresponding predictions given by full-wave simulations of the MSs that results in fairly good agreement with experimental findings.

As in the previous case, these MSs display an onset of plasmonic resonances in correspondence of $f^1_{x,y}\ c/P_{x,y}\sqrt{\varepsilon^{'}_d}$. From the tabulated x- and y- periodicity of MS1 and MS2 one can easily get $f^1_{x,y}(MS1) = 0.46, 0.70THz$ and $f^1_{x,y}(MS2) = 0.46, 1.10THz$, in full agreement with experimental results.

Differently from the MGs, the MSs show – because of the inherent asymmetry in the respective UC geometry - a different periodicity and a significant change in transmission for the two polarizations, the more the larger is the lateral size difference.

The variation observed in the transmission for the two polarizations stimulates an interest in applications where a large change is needed according to the signal polarization. For example, we record at 0.44 THz a variation $\Delta T = |T_y(MS2) - T_x(MS2)| = 24dB$ for MS2, while a similar value, 19 dB, is observed for MS1 at 0.53 THz. Such a variation in transmission can be employed to realize THz signal decoders, engineering MSs to introduce at specific frequencies a light polarization control through switchable $\lambda/2$ plate [36].

Lastly, devices realized with the FLA approach can be easily used for the development of sensing platforms. The structures we have presented, in fact, introduce a comb-like transmission where changes in resonance positions can be accurately mapped varying the dielectric constant of the analyte [37].

To summarize, we have exploited FLA of an Au metallic layer over a Si substrate to realize a number of simple MSs operating in the THz regime. Two processing modes were used obtaining MSs either by creating patterns of through holes in the metallic film or by generating an array of Au islands by selective removal of the Au film. The good control on the fabrication process and the full match of the THz response of the fabricated MSs with electromagnetic simulations render their production by FLA a promising approach towards the design of optical devices with robust and superior performances. For example, novel components with very high quality factors and significant polarization control can be developed. In addition, even if the elaborated MSs are composed by rather simple patterns, our findings demonstrate the feasibility of the FLA approaches for the elaboration of THz metasurfaces, which can surely benefit in the near future by the recent development of laser surface processing with complex, structured laser beams [38,39].

CRediT authorship contribution statement

Gian Paolo Papari: Conceptualization, Methodology, Writing - original draft. **Jijil J.J. Nivas:** Investigation. **Can Koral:** Data curation, Formal analysis. **Elaheh Allahyari:** Resources. **Salvatore Amoruso:** Visualization, Writing - review & editing. **Antonello Andreone:** Supervision, Writing - review & editing.

Declaration of Competing Interest

The authors declare that they have no known competing financial interests or personal relationships that could have appeared to influence the work reported in this paper.

Acknowledgments

This work has been partially supported by the National Institute for Nuclear Physics (INFN) under the project "Terahertz ERA".

References

[1] C.M. Soukoulis, M. Wegener, Past achievements and future challenges in the development of three-dimensional photonic metamaterials, Nat. Photonics. 5 (2011) 523–530, https://doi.org/10.1038/nphoton.2011.154.
[2] S. Zhu, X. Zhang, Metamaterials: artificial materials beyond nature, 131–131, Natl.

Sci. Rev. 5 (2018), https://doi.org/10.1093/nsr/nwy026.
[3] A.M. Urbas, Z. Jacob, L.D. Negro, N. Engheta, A.D. Boardman, P. Egan, A.B. Khanikaev, V. Menon, M. Ferrera, N. Kinsey, C. DeVault, J. Kim, V. Shalaev, A. Boltasseva, J. Valentine, C. Pfeiffer, A. Grbic, E. Narimanov, L. Zhu, S. Fan, A. Alù, E. Poutrina, N.M. Litchinitser, M.A. Noginov, K.F. MacDonald, E. Plum, X. Liu, P.F. Nealey, C.R. Kagan, C.B. Murray, D.A. Pawlak, I.I. Smolyaninov, V.N. Smolyaninova, D. Chanda, Roadmap on optical metamaterials, J. Opt. 18 (2016) 093005, , https://doi.org/10.1088/2040-8978/18/9/093005.
[4] R. Singh, W. Cao, I. Al-naib, L. Cong, W. Withayachumnankul, W. Zhang, Ultrasensitive terahertz sensing with high-Q Fano resonances in metasurfaces Ultrasensitive terahertz sensing with high- Q Fano resonances in metasurfaces, Appl. Phys. Lett. 105 (2014) 1–5, https://doi.org/10.1063/1.4895595.
[5] M.R.M. Hashemi, S.H. Yang, T. Wang, N. Sepúlveda, M. Jarrahi, Electronically-controlled beam-steering through vanadium dioxide metasurfaces, Sci. Rep. 6 (2016) 1–8, https://doi.org/10.1038/srep35439.
[6] J.B. Pendry, Negative refraction makes a perfect lens, Phys. Rev. Lett. 85 (2000) 3966–3969, https://doi.org/10.1103/PhysRevLett.85.3966.
[7] S.C. Jiang, X. Xiong, Y.S. Hu, Y.H. Hu, G. Bin Ma, R.W. Peng, C. Sun, M. Wang, Controlling the polarization state of light with a dispersion-free metastructure, Phys. Rev. X. 4 (2014) 1–6, https://doi.org/10.1103/PhysRevX.4.021026.
[8] A. Alù, M.G. Silveirinha, A. Salandrino, N. Engheta, Epsilon-near-zero metamaterials and electromagnetic sources: Tailoring the radiation phase pattern, Phys. Rev. B - Condens. Matter Mater. Phys. 75 (2007) 1–13, https://doi.org/10.1103/PhysRevB.75.155410.
[9] G.P. Papari, C. Koral, A. Andreone, Geometrical dependence on the onset of surface plasmon polaritons in THz grid metasurfaces, Sci. Rep. 9 (2019) 1–12, https://doi.org/10.1038/s41598-018-36648-x.
[10] J.E. Heyes, W. Withayachumnankul, N.K. Grady, D.R. Chowdhury, A.K. Azad, H.-T. Chen, Hybrid metasurface for ultra-broadband terahertz modulation, Appl. Phys. Lett. 105 (2014) 181108, , https://doi.org/10.1063/1.4901050.
[11] S. Walia, C.M. Shah, P. Gutruf, H. Nili, D.R. Chowdhury, W. Withayachumnankul, M. Bhaskaran, S. Sriram, Flexible metasurfaces and metamaterials: A review of materials and fabrication processes at micro- and nano-scales, Appl. Phys. Rev. 2 (2015), https://doi.org/10.1063/1.4913751.
[12] R. Mendis, A.J. Taylor, A. Benz, H.O. Everitt, I. Brener, J.L. Reno, N. Karl, D.M. Mittleman, M.S. Heimbeck, H.-T. Chen, Characterization of an active metasurface using terahertz ellipsometry, Appl. Phys. Lett. 111 (2017) 191101, , https://doi.org/10.1063/1.5004194.
[13] Z. Song, M. Wei, Z. Wang, G. Cai, Y. Liu, Y. Zhou, Terahertz absorber with reconfigurable bandwidth based on isotropic vanadium dioxide metasurfaces, IEEE Photonics J. 11 (2019) 1–7, https://doi.org/10.1109/JPHOT.2019.2898981.
[14] S. Savo, E. Di Gennaro, A. Andreone, Superlensing properties of one-dimensional dielectric photonic crystals, Opt. Express. 17 (2009) 19848, https://doi.org/10.1364/oe.17.019848.
[15] I. Anghel, F. Jipa, A. Andrei, S. Simion, R. Dabu, A. Rizea, M. Zamfirescu, Femtosecond laser ablation of TiO2 films for two-dimensional photonic crystals, Opt. Laser Technol. 52 (2013) 65–69, https://doi.org/10.1016/j.optlastec.2013.04.020.
[16] Y. Zhang, M. Yuan, L. Chen, B. Cai, R. Yang, Y. Zhu, Broadband terahertz anti-reflective structure fabricated by femtosecond laser drilling technique, Opt. Commun. 361 (2016) 148–152, https://doi.org/10.1016/j.optcom.2015.10.051.
[17] G. Papari, G. Testa, R. Bernini, A. Andreone, A PDMS photonic crystal slab for THz sensing, 2016 10th Int Congr. Adv. Electromagn. Mater. Microwaves Opt. Metamaterials 2016 (2016) 274–276, https://doi.org/10.1109/MetaMaterials.2016.7746514.
[18] E. Di Gennaro, D. Morello, C. Miletto, S. Savo, A. Andreone, G. Castaldi, V. Galdi, V. Pierro, A parametric study of the lensing properties of dodecagonal photonic quasicrystals, Photonics Nanostructures - Fundam. Appl. 6 (2008) 60–68, https://doi.org/10.1016/j.photonics.2007.12.001.
[19] P.T. Rose, E. Di Gennaro, G. Abbate, A. Andreone, Isotropic properties of the photonic band gap in quasicrystals with low-index contrast, Phys. Rev. B - Condens. Matter Mater. Phys. 84 (2011) 1–7, https://doi.org/10.1103/PhysRevB.84.125111.
[20] R. Gente, I. Al-Naib, M. Koch, N. Born, Laser beam machined free-standing terahertz metamaterials, Electron. Lett. 51 (2015) 1012–1014, https://doi.org/10.1049/el.2015.0655.
[21] M.L. Tseng, P.C. Wu, S. Sun, C.M. Chang, W.T. Chen, C.H. Chu, P.L. Chen, L. Zhou, D.W. Huang, T.J. Yen, D.P. Tsai, Fabrication of multilayer metamaterials by femtosecond laser-induced forward-transfer technique, Laser Photonics Rev. 6 (2012) 702–707, https://doi.org/10.1002/lpor.201200029.
[22] B. Voisiat, A. Bičiunas, I. Kašalynas, G. Račiukaitis, Band-pass filters for THz spectral range fabricated by laser ablation, Appl. Phys. A Mater. Sci. Process. 104 (2011) 953–958, https://doi.org/10.1007/s00339-011-6456-3.
[23] M. Zamfirescu, R. Dabu, M. Dumitru, G. Sajin, F. Craciunoiu, Femtosecond laser fabrication of metamaterials for high frequency microwave devices, J. Laser Micro Nanoeng. 3 (2008) 5–8, https://doi.org/10.2961/jlmn.2008.01.0002.
[24] A. Mekys, L. Minkevičius, G. Račiukaitis, V. Tamošiu¯nas, R. Venckevičius, I. Kašalynas, B. Voisiat, D. Seliuta, G. Valušis, Terahertz zone plates with integrated laser-ablated bandpass filters, Electron. Lett. 49 (2013) 49–50, https://doi.org/10.1049/el.2012.3509.
[25] S.I. Kudryashov, P.A. Danilov, A.P. Porfirev, I.N. Saraeva, T.H.T. Nguyen, A.A. Rudenko, R.A. Khmelnitskii, D.A. Zayarny, A.A. Ionin, A.A. Kuchmizhak, S.N. Khonina, O.B. Vitrik, High-throughput micropatterning of plasmonic surfaces by multiplexed femtosecond laser pulses for advanced IR-sensing applications, Appl. Surf. Sci. 484 (2019) 948–956, https://doi.org/10.1016/j.apsusc.2019.04.048.
[26] D. Pavlov, S. Gurbatov, S.I. Kudryashov, P.A. Danilov, A.P. Porfirev, S.N. Khonina, O.B. Vitrik, S.A. Kulinich, M. Lapine, A.A. Kuchmizhak, 10-million-elements-per-second printing of infrared-resonant plasmonic arrays by multiplexed laser pulses, Opt. Lett. 44 (2019) 283, https://doi.org/10.1364/ol.44.000283.
[27] K. Sakoda, ed., Electromagnetic Metamaterials, Modern Insights into Macroscopic Electromagnetic Fields, 2019th ed., Springer Singapore, n.d. http://doi.org/10.1007/978-981-13-8649-7.
[28] J.B. Pendry, Mimicking surface plasmons with structured surfaces, Science 305 (5685) (2004) 847–848, https://doi.org/10.1126/science:1098999.
[29] L. Martin-Moreno, F.J. Garcia-Vidal, H.J. Lezec, K.M. Pellerin, T. Thio, J.B. Pendry, T.W. Ebbesen, Theory of extraordinary optical transmission through subwavelength hole arrays, Phys. Rev. Lett. 86 (2001) 1114–1117, https://doi.org/10.1103/PhysRevLett.86.1114.
[30] T.W. Ebbesen, H.J. Lezec, H.F. Ghaemi, T. Thio, P.A. Wolff, T. Thio, P.A. Wolff, Extraordinary optical transmission through sub-wavelength hole arrays, Nature 86 (1998) 1114–1117, https://doi.org/10.1038/35570.
[31] W.L. Barnes, A. Dereux, T.W. Ebbesen, Surface plasmon subwavelength optics, Nature 424 (2003) 824–830, https://doi.org/10.1038/nature01937.
[32] D.R. Smith, J.B. Pendry, Homogenization of metamaterials by field averaging (invited paper), J. Opt. Soc. Am. B. 23 (2006) 391, https://doi.org/10.1364/JOSAB.23.000391.
[33] J.J.D. Joannopoulos, S. Johnson, J.N.J. Winn, R.R.D. Meade, Photonic crystals: molding the flow of light, Princeton University Press, 41 William Street, Princeton, New Jersey 08540, 2008. doi:10.1063/1.1586781.
[34] G. Scalari, C. Maissen, S. Cibella, R. Leoni, J. Faist, High quality factor, fully switchable terahertz superconducting metasurface, Appl. Phys. Lett. 105 (2014) 261104, , https://doi.org/10.1063/1.4905199.
[35] C. Jansen, I.A.I. Al-Naib, N. Born, M. Koch, Terahertz metasurfaces with high Q-factors, Appl. Phys. Lett. 98 (2011), https://doi.org/10.1063/1.3553193.
[36] Y. Nakata, Y. Taira, T. Nakanishi, F. Miyamaru, Freestanding transparent terahertz half-wave plate using subwavelength cut-wire pairs, Opt. Express. 25 (2017) 2107, https://doi.org/10.1364/oe.25.002107.
[37] Gian Paolo Papari, Can Koral, Antonello Andreone, Encoded-enhancement of THz metasurface figure of merit for label-free sensing, Sensors 19 (11) (2019) 1–9, https://doi.org/10.3390/s19112544.
[38] J.J. Nivas, F. Cardano, Z. Song, A. Rubano, R. Fittipaldi, A. Vecchione, D. Paparo, L. Marrucci, R. Bruzzese, S. Amoruso, Surface structuring with polarization-singular femtosecond laser beams generated by a q-plate, Sci. Rep. 7 (2017) 1–10, https://doi.org/10.1038/srep42142.
[39] J. Jj Nivas, E. Allahyari, F. Cardano, A. Rubano, R. Fittipaldi, A. Vecchione, D. Paparo, L. Marrucci, R. Bruzzese, S. Amoruso, Surface structures with unconventional patterns and shapes generated by femtosecond structured light fields, Sci. Rep. 8 (2018) 1–11, https://doi.org/10.1038/s41598-018-31768-w.